Thermal Decomposition Mechanism of Tetraethylsilane by Flash Pyrolysis Vacuum Ultraviolet Photoionization Mass Spectrometry and DFT Calculations: The Competition Between *β*-hydride Elimination and Bond Homolysis

Kuanliang Shao [a], Xinghua Liu,[b] and Jingsong Zhang [a*]

[a] Department of Chemistry, University of California, Riverside, California 92521, United States.

[b] Current address: School of Science, Hainan University, Hainan 570228, China.

[*] Email: jingsong.zhang@ucr.edu; Also at Air Pollution Research Center, University of California, Riverside, California 92521, United States.

Abstract

Thermal decomposition of tetraethylsilane was investigated at temperatures up to 1330 K using flash pyrolysis vacuum ultraviolet photoionization mass spectrometry. Density functional theory and transition state theory calculations were performed to corroborate the experimental observations. Both experimental and theoretical evidence showed that the pyrolysis of tetraethylsilane was initiated by Si-C bond fission to the primary reaction products, triethylsilyl ($SiEt_3$) and ethyl radicals. In the secondary reactions of the triethylsilyl radical, at lower temperatures, *β*-hydride elimination pathway (producing $HSiEt_2$) was found to be more favored than its competing reaction channel, Si-C bond fission (producing $SiEt_2$); as the temperature further increased, the Si-C bond fission reaction became significant. Other important secondary reaction products, such as $EtHSi{=}CH_2$ (m/z = 72), H_2SiEt (m/z = 59), and SiH_3 (m/z = 31) were identified, and their formation mechanisms were also proposed.

Key words: mass spectrometry; density functional theory; pyrolysis; tetraethylsilane

Introduction

Silicon carbide (SiC) thin film, due to its excellent performance in physical, chemical, and electronic properties, has been widely applied in the electronic industry.[1-4] Using organosilanes as a single source precursor for the SiC thin film production in chemical vapor deposition (CVD) has become an improvement initiative.[5-10] Compared to using separate carbon and silicon precursors, using single source organosilanes precursor, as the Si-C bond already exists, could avoid high temperature which is required for the formation of Si-C bond in gas phase between the carbon and silicon precursors, and therefore, reduce the mismatches between Si and SiC in lattice constants and thermal expansion coefficients.[8, 11] A number of organosilanes have been regarded as good candidates for CVD production of SiC;[12] among them, tetraethylsilane ($SiEt_4$) has been considered as a popular precursor in various investigations of SiC thin film productions using the CVD method.[12-19]

Amjoud et al. studied the metal-organic CVD of tetraethylsilane at 500 – 1000 °C in a classical horizontal CVD reactor interfaced with gas-phase chromatograph.[16] It was found that thermal decomposition of tetraethylsilane started at 845 °C in helium carrier gas and C_2H_4 was a major product in the gas-phase reactions. However, a detailed gas-phase reaction mechanism was not proposed. Pola et al. explored ArF laser photolysis of tetraethylsilane at 193.3 nm for its suitability for use in CVD of Si/C materials and examined the products using FTIR spectroscopy.[20] It was reported that the only initiation pathway in the photolytic decomposition of tetraethylsilane is β-hydride elimination of ethylene (reaction (1)), and the produced $HSiEt_3$ would further undergo stepwise ethylene elimination reactions until the formation of SiH_4 (reaction (2)). However, it was also noted that the presumed key intermediates H_2SiEt_2, H_3SiEt, and SiH_4 were not detected.

$$SiEt_4 \xrightarrow{h\nu \text{ at } 193 \text{ nm}} HSiEt_3 + C_2H_4 \quad (1)$$

$$HSiEt_3 \xrightarrow{\text{multistep photolysis at 193 nm}} SiH_4 + 3C_2H_4 \quad (2)$$

The β-hydride elimination mechanism was also found in the pyrolysis of ethylsilane (H_3SiEt), a simple homolog of tetraethylsilane ($SiEt_4$). The thermal decomposition mechanism of ethylsilane (H_3SiEt) has been investigated by several researchers.[21-24] Ring et al. and Rickborn et al. studied the thermal decomposition of H_3SiEt using a single-pulse shock tube at temperatures between 1080 K and 1245 K.[21, 22] They proposed that the thermal decomposition of H_3SiEt did not undergo the direct β-hydride elimination of ethylsilane (reaction (3)); instead, it was primarily initiated by an H_2 elimination channel (reaction (4)). The produced reactive intermediate, HSiEt, further dissociated via a β-hydride elimination channel to SiH_2 and C_2H_4 (reaction (5)). Jardine et al. studied the thermal decomposition of ethylsilane in a static cell,[23, 25] and Sela et al. later revisited the thermal decomposition of ethylsilane using a single-pulse shock tube;[24] their results were mostly in agreement with the initiation reaction of H_3SiEt and its subsequent dissociation reactions proposed by Ring et al. and Rickborn et al.[21, 22] The gas-phase pyrolysis study on other ethylsilanes, diethylsilane, triethylsilane, and tetraethylsilane, have been limited. The β-hydride elimination reaction of the surface SiEt group producing ethylene and SiH on the surface (reaction (6)) is a tool to quantitatively explore the adsorption and decomposition of ethylsilanes (H_xSiEt_{4-x}) on the surface.[12, 26-29] Nevertheless, the fundamentals of the β-hydride elimination mechanism of the SiEt group is less studied in the gas phase. Tetraethylsilane would be an ideal candidate to investigate the β-hydride elimination reaction of the SiEt group in the gas phase, as it does not possess an active Si-H bond and the initial reaction mechanism could be less complicated.[12]

$$H_3SiEt \rightarrow SiH_4 + C_2H_4 \quad (3)$$

$$H_3SiEt \rightarrow HSiEt + H_2 \quad (4)$$

$$HSiEt \rightarrow SiH_2 + C_2H_4 \quad (5)$$

$$Si\text{-}C_2H_5(ad) \rightarrow SiH\,(ad) + C_2H_4 \quad (6)$$

To further explore the gas-phase decomposition mechanism of tetraethylsilane and its adequacy for CVD, and to better understand the *β*-hydride elimination mechanism of the SiEt group in the gas phase, flash pyrolysis of tetraethylsilane ($SiEt_4$) was studied using vacuum ultraviolet photoionization time-of-flight mass spectrometry (VUV-PI-TOF-MS) in this work. Density functional theory (DFT) calculations of the energetics of the reactants, transition states, and products were carried out to identify the competing reaction pathways. Furthermore, transition state theory (TST)/variational transition state theory (VTST) calculations were performed, and the rate constants of various unimolecular decomposition pathways were compared to illustrate the competitions between the *β*-hydride elimination and the bond homolysis reactions.

Experimental and computational methods

The thermal decomposition study of tetraethylsilane was conducted using a home-made flash pyrolysis vacuum ultraviolet photoionization time-of-flight mass spectrometer (VUV-PI-TOFMS), which has been described previously.[30-35] The design of the flash pyrolysis microreactor was similar to that reported by Chen and co-workers.[36] The tetraethylsilane sample was purchased from Sigma Aldrich (99 %). The precursor was introduced in the apparatus by bubbling helium carrier gas through the liquid tetraethylsilane sample; the total backing pressure of the gas mixture was around 950 torr, while the precursor was diluted to ~ 0.5 % in the gas phase. The concentration of the tetraethylsilane precursor in the gas mixture was calculated based on the assumption that the vaporization and condensation of the precursor were in equilibrium over the liquid phase. The

gas mixture then expanded into a SiC microreactor (Carborundum, 2 mm o.d., 1 mm i.d.) after passing thorough a pulse valve. The pyrolysis of the precursor took place in the heated region (10 mm length) of the SiC microreactor which was heated resistively by electric currents that flew through. The temperature was monitored by a type C thermocouple which was attached to the outside surface of the microreactor and was calibrated to the inside temperature of the microreactor. According to Guan et al. and Zagidullin et al., the residence time within the heated region was estimated to be less than 100 μs in this work.[37, 38] Based on Zagidullin et al., the average pressure within the heated region in the microreactor was estimated to be 10 torr.[38] The reaction conditions within the microreactor significantly favored unimolecular reactions, while bimolecular reactions and wall reactions were reduced.[35, 37-39] After exiting the nozzle, the gas mixture, which contained the products, reactive intermediates, and unreacted reactants, supersonically expanded into the main chamber. After being selected by a skimmer, the isolated molecular beam was intercepted by 118 nm VUV radiation in the photoionization region. The 118 nm radiation was generated by tripling the 355 nm radiation from an Nd:YAG laser in a xenon cell (with ~18 torr of xenon). The reactive intermediates, products, and unreacted reactants in the molecular beam were photoionized. The ion signals were then detected and recorded using a digital oscilloscope (Tektronix TDS3032) after averaging over 512 laser shots at each SiC microreactor temperature.

Density functional theory (DFT) calculations on the geometries and energetics of corresponding transition states, intermediates, products, and reactants were performed using the Gaussian 16 package.[40] All geometries including transition states were optimized using the UB3LYP method under 6-31+G(d,p) basis sets. This method was chosen as it has been reported that the B3LYP method provides good results in geometry optimization while maintaining computational efficiency, and the unrestricted method was employed to ensure the consistency

between the open-shell and closed-shell calculations.[41, 42] A scaling factor of 0.964 was applied to all the zero-point energies, as recommended by the Computational Chemistry Comparison and Benchmark DataBase (CCCBDB). The single-point energy for each species were calculated at the UM06-2X/6-311++G(3df, 2pd) level of theory.[43] The M06-2X method could produce good thermal chemistry calculation results for main group compounds with a reasonable computational cost.[44] Transition states with only one imaginary frequency were tested using intrinsic reaction coordinate (IRC) calculations at the UB3LYP/6-31+G(d,p) level. The geometries of the species involved could be located in the Supporting Information (SI). All results are presented as relative energies at 0 Kelvin (ΔE_{0K}).

Unimolecular reaction rate constants of the tetraethylsilane ($SiEt_4$) dissociation channels, and the secondary dissociation channels of the triethylsilyl radical ($SiEt_3$) were calculated using transition state theory (TST) and variational transition state theory (VTST). For the unimolecular dissociation reaction with a conventional transition state, the rate constant was calculated using TST with Wigner tunneling correction at various temperatures.[45-48] The frequency analysis of reactants and transition states were evaluated at the UB3LYP/6-31+G(d,p) level of theory with a recommended scaling factor,[49] while the single point energy calculations were carried out at the UM06-2X/6-311++G(3df, 2pd) level of theory as described earlier. For the barrierless bond fission reactions, VTST with Wigner tunneling correction was used.[45-48, 50] A series of constrained optimizations along the reaction path were carried out, and at each optimized geometry ("trial transition state"), the potential energy and vibrational frequencies were calculated. The dividing surface for the barrierless reactions at different temperatures were determined by finding the maximum Gibbs free energy change $\Delta G^{o}(T)$ of the "trial transition state" along the reaction pathway at various temperatures.[50, 51] The geometries and vibrational frequencies of the reactants,

transition states, and selected "trial transition state" are summarized in SI. All rate constant calculations were performed utilizing the KISTHELP package.[47, 52, 53]

Results and discussions

The mass spectra of the tetraethylsilane pyrolysis at temperatures between 300 K and 1330 K are displayed in Figure 1. At 300 K, the signal of m/z = 144 and 145 represented the parent molecule tetraethylsilane ($SiEt_4$). The relative abundance for ^{28}Si, ^{29}Si, and ^{30}Si are 92.2 %, 4.7 %, and 3.1 %, respectively.[54] The relative abundance of ^{12}C and ^{13}C are 98.9 % and 1.01 %. The ratio of peak area of m/z = 145 to m/z = 144 was determined to be 0.19 in Figure 1, close to the theoretical value of 0.14. Other peaks at 300 K, such as m/z = 115 and 116 ($SiEt_3$), m/z = 87 ($HSiEt_2$), and m/z = 141 were caused by dissociative photoionization of the parent molecule.

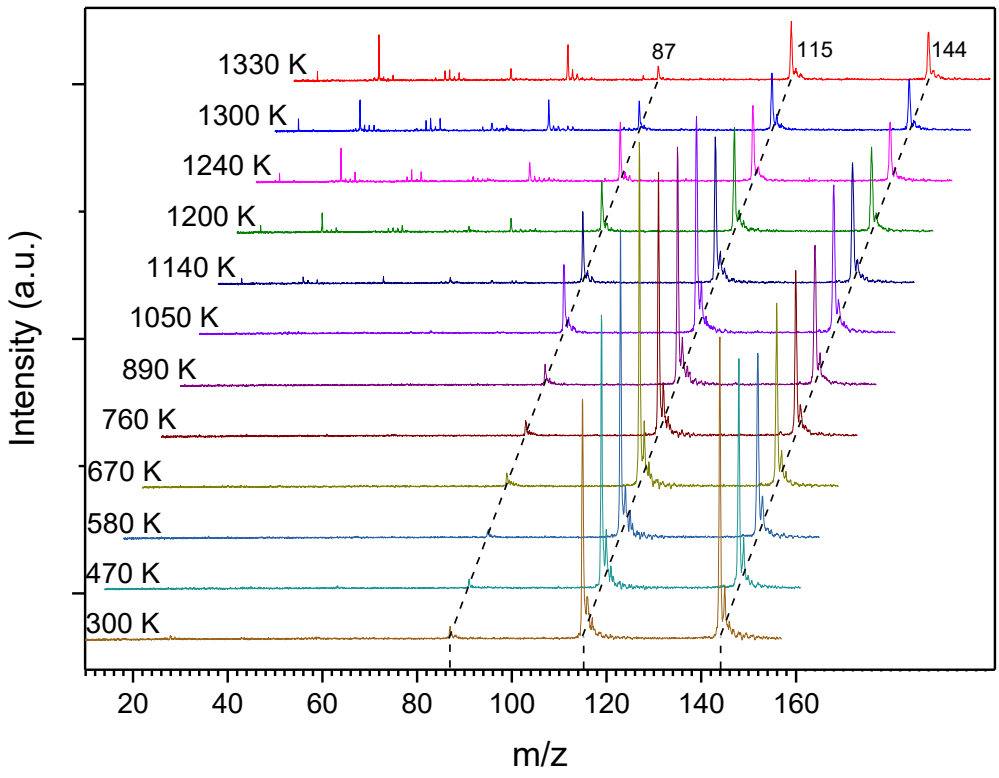

Figure 1. Mass spectra of the tetraethylsilane pyrolysis at 300 K to 1330 K. The mass spectra are offset horizontally and vertically for clarity.

1. The initiation step of the tetraethylsilane pyrolysis.

Similar to the thermal decomposition of the related organosilane molecule tetramethylsilane ($SiMe_4$),[33, 55] the Si-C bond fission (reaction (7)) was considered the initiation step in the tetraethylsilane pyrolysis. As shown in Figure 1 and Figure 2, the signal of m/z = 115, which corresponds to $SiEt_3$, was observed at 300 K as a dissociative photoionization peak of the parent molecule. As the temperature increased, its peak intensity increased and then started to decrease above 1050 K. Both dissociative photoionization and thermal decomposition of the parent molecule can contribute to the peak area of the fragment peak. At low temperatures, the fragment peak was only due to the dissociative photoionization; as the temperature increased beyond the decomposition onset temperature, the thermal decomposition started to contribute to the fragment peak. Consequently, as shown in Li et al. and Shao et al,[34, 55] plotting the ratio of the fragment peak

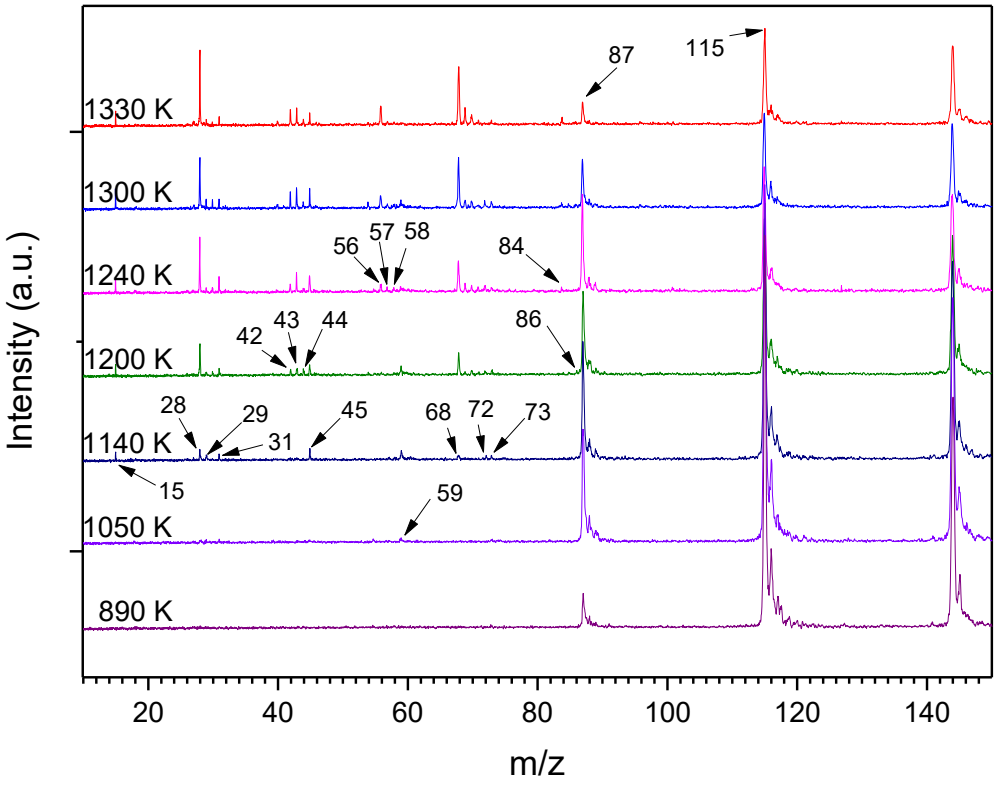

Figure 2. Enlarged mass spectra of the tetraethylsilane pyrolysis from 890 K to 1330 K. The mass spectra are offset vertically for clarity.

area to the parent peak area is a useful method to determine the temperature at which the thermal decomposition reaction starts. However, the peak area ratio of m/z 115 vs. m/z 144 was 0.86 at 300 K, which was large due to the prominent contribution to m/z 115 from dissociative photoionization of the parent molecule and hindered the determination of the additional contribution from thermal decomposition at elevated temperatures.[34] Instead, the peak area ratio of m/z 87 vs. m/z 144 is plotted in Figure 3 to determine the onset temperature for reaction (7). $SiEt_3$ was the product of the primary reaction (7), and, as will be discussed later, it could promptly decompose into $HSiEt_2$ (m/z = 87) and C_2H_4 via a two-step mechanism (reaction (8)). The production of $HSiEt_2$ (m/z = 87), as the immediate secondary decomposition product of $SiEt_3$, could suggest the upper limit of the onset temperature of reaction (7). According to Figure 3, the peak area ratio of m/z 87 vs. m/z 144 increased initially around 890 K and then significantly around 1050 K, and the ratio dropped when it reached its maximum at 1240 K. The co-product of $SiEt_3$ in

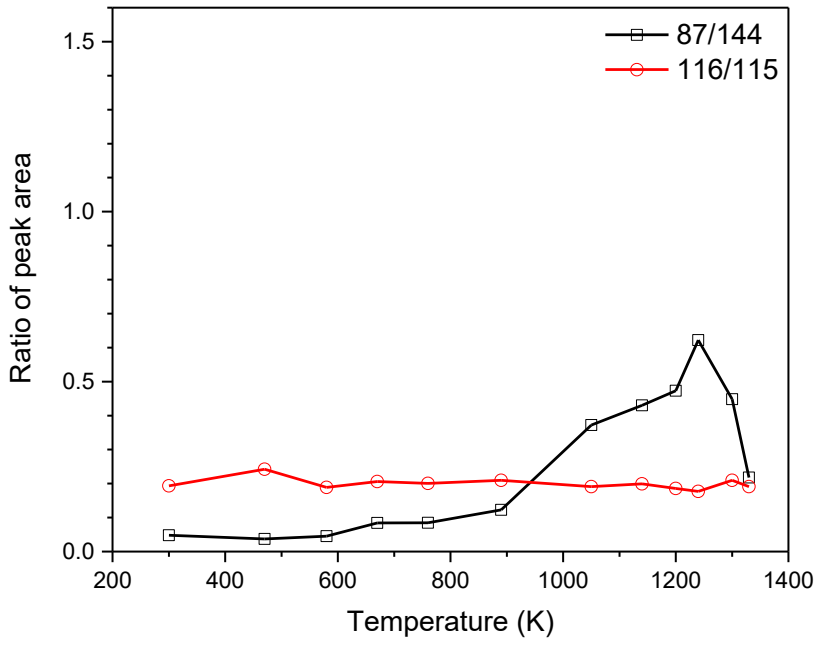

Figure 3. The plot of the m/z = 87 peak area over m/z = 144 peak area, and the m/z = 116 peak area over m/z = 115 peak area in the temperature range from 300 K to 1330 K.

reaction (7), C_2H_5 (m/z = 29), was first detected at 1050 K. Its peak intensity increased with increasing temperature until 1300 K, and then it started to decrease. These could serve as direct evidence that reaction (7) was initiated around 1050 K. From the discussions above, it is considered that the onset temperature for the Si-C bond homolysis reaction (reaction (7)) was around 1050 K.

$$SiEt_4 \rightarrow SiEt_3 + C_2H_5 \quad (7)$$

$$SiEt_3 \rightarrow HSiEt_2C_2H_4 \rightarrow HSiEt_2 + C_2H_4 \quad (8)$$

The β-hydride elimination mechanism of tetraethylsilane (reaction (9)) was not experimentally observed in the initiation step. The possible products of reaction (9) are triethylsilane ($HSiEt_3$) and ethylene (C_2H_4). In Figure 1 and 2, the signal of $HSiEt_3$ (m/z = 116) overlapped with one of the isotopic signals of $SiEt_3$. The peak area ratio of m/z 116 vs. m/z 115 is plotted in Figure 3 in order to identify the production of $HSiEt_3$. However, the curve remained flat as the temperature increased, reflecting the peak area ratio of the m/z 116 and m/z 115 isotope peaks in $SiEt_3$ and indicating little or no production of $HSiEt_3$ from thermal decomposition at all the temperatures. The signal of C_2H_4, the possible co-product of $HSiEt_3$ in reaction (9), was first observed at 1140 K as shown in Figure 2; however, it could be produced from the fast H-loss reaction of C_2H_5 (produced in reaction (7)) or reaction (8) instead.[56, 57]

$$SiEt_4 \rightarrow HSiEt_3 + C_2H_4 \quad (9)$$

The β-hydride elimination mechanism of tetraethylsilane was also not supported by the theoretical calculations. The quantum chemistry calculations regarding the energetics of the possible initiation channels are displayed in Figure 4 (the geometry of the species involved could be found in the SI Section 1 and 2). The calculated energy threshold for the Si-C bond homolysis

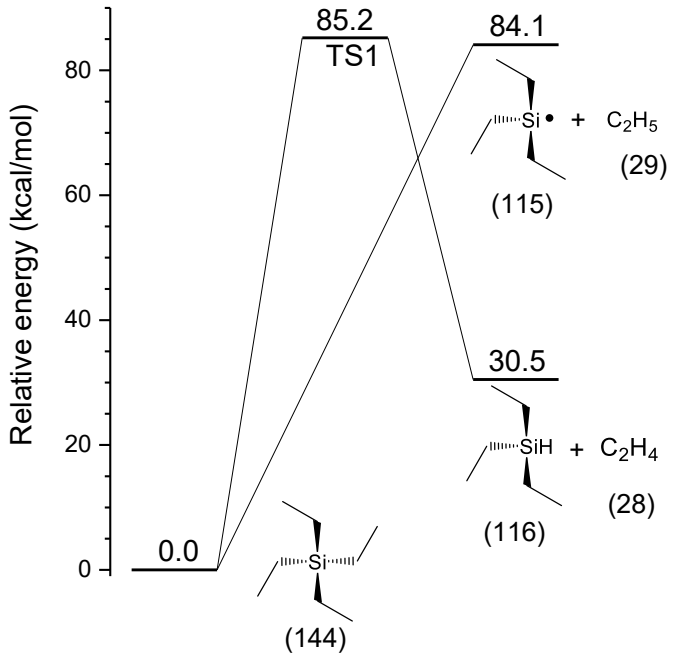

Figure 4. Energetics (0 K) of the possible initiation channels for the pyrolysis of tetraethylsilane at the UM06-2X/6-311++G(3df, 2pd)//UB3LYP/6-31+G(d,p) level.

reaction (7) was 84.1 kcal/mol, while the calculated energy barrier for the *β*-hydride elimination channel via TS1 was 85.2 kcal/mol. The Si-C bond homolysis reaction is energetically slightly favored than the *β*-hydride elimination channel, and furthermore it has a loose transition state than the tight transition state of the molecular elimination pathway. Kinetic analysis was performed by the VTST calculation for the bond homolysis channel and the TST calculation for the molecular elimination via TS1. The unimolecular reaction rate constant calculations for the initiation channels are summarized in Figure 5 (the details for the VTST/TST calculations, such as the frequencies of the transition states, could be found in the SI Section 3 and 4). It shows that the rate constant for the Si-C bond fission channel is much larger than that for the *β*-hydride elimination channel. For example, at the onset temperature of reaction (7), 1050 K, the calculated unimolecular rate constant of reaction (7) is 0.13 s^{-1}, while that of reaction (9) is 9.2×10^{-7} s^{-1}. This rate constant

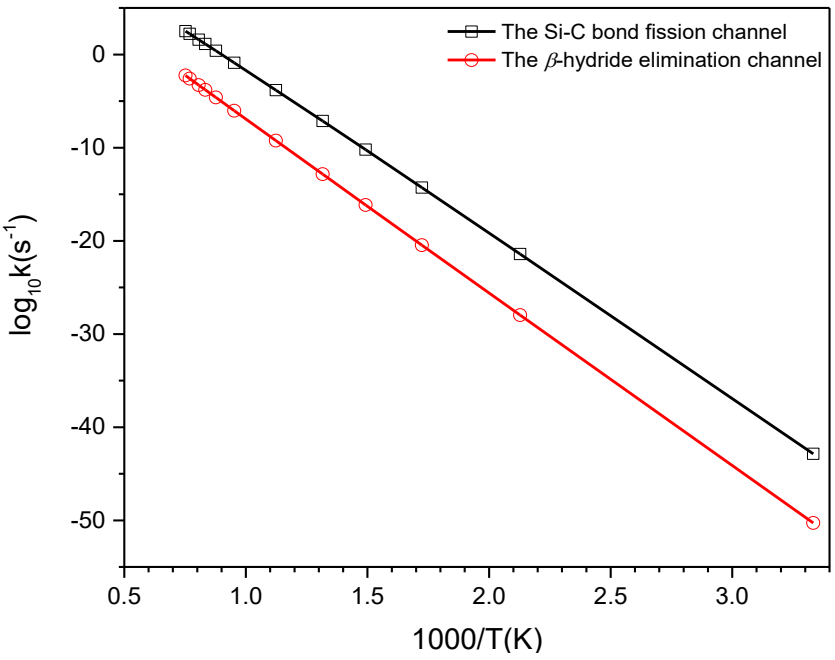

Figure 5. Unimolecular rate constant calculations of the initiation reactions with the TST/VTST method. The results are displayed in the form of $\log_{10}k$ vs 1000/T.

comparison demonstrates that the Si-C bond fission reaction is much more competitive than the β-hydride elimination reaction in the initiation step.

2. Secondary reactions of the triethylsilyl radical.

The secondary reaction of the trimethylsilyl radical, which was the predominant product in the initiation step, was mostly advanced by the β-hydride elimination mechanism. As mentioned earlier, the appearance of the m/z = 87 peak ($HSiEt_2$) was used as the evidence to identify the production of the triethylsilyl radical. In Figure 1 and 2, the signal of the m/z = 87 peak started to increase significantly at around 1050 K. The signal of the counterpart of $HSiEt_2$ in reaction (8), C_2H_4 (m/z = 28), was first found at 1140 K, and its intensity kept increasing with the temperature. C_2H_4 (m/z = 28) was not observed simultaneously at 1050 K, possible because its ionization

potential (10.51 eV[58]) is slightly higher than the VUV photon energy (10.49 eV) which made the detection of the C_2H_4 signal difficult.[32] Figure 3 also shows the trend of the peak ratio of m/z 87 vs. m/z 144 as a function of temperature, indicating that thermal decomposition contribution to the m/z = 87 peak became significant at around 1050 K. On the other hand, the Si-C bond homolysis of the triethylsilyl radical (reaction (10)) was found to be insignificant. As shown in Figure 1 and 2, the signal of $:SiEt_2$ (m/z = 86) first appeared at 1200 K with a very small intensity, and as the temperature further increased, the m/z =86 signal disappeared. In the mass spectra (Figure 1 and 2), m/z = 100 and 114 peaks were not observed at all the elevated temperature, indicating the absense of β-sicssion pathways of $SiEt_3$, $Et_2Si{=}CH_2$ (m/z 100) + CH_3 and $Et_2Si{=}CHCH_3$ (m/z =114) + H. This was consistent with the fact that the formation of the Si=C bond (in both $Et_2Si{=}CH_2$ and $Et_2Si{=}CHCH_3$) is energetically less favorable than the formation of the C=C bond (in C_2H_4 in the main pathway, reaction (8)).

$$SiEt_3 \rightarrow SiEt_2 + C_2H_5 \qquad (10)$$

To illuminate the β-hydride elimination mechanism of the triethylsilyl radical, and compare the energetics of several competing reaction channels, quantum chemistry calculations regarding dissociations of $SiEt_3$ were carried out, and the results are displayed in Figure 6. The theoretical calculations indicated that the β-hydride elimination reaction of $SiEt_3$ proceeds via a two-step pathway. $SiEt_3$ first isomerizes to an intermediate ($HSiEt_2C_2H_4$) via TS2 with an energy barrier of 37.5 kcal/mol. Then it readily decomposes into $HSiEt_2$ and C_2H_4 via TS3, with an energy barrier of 24.9 kcal/mol with respect to $HSiEt_2C_2H_4$ (reaction (8)). The overall energy barrier for the β-hydride elimination of $SiEt_3$ is 37.5 kcal/mol. The energy threshold for its competing reaction channel, the Si-C bond cleavage producing $:SiEt_2$ and C_2H_5, is calculated to be 60.8 kcal/mol. It

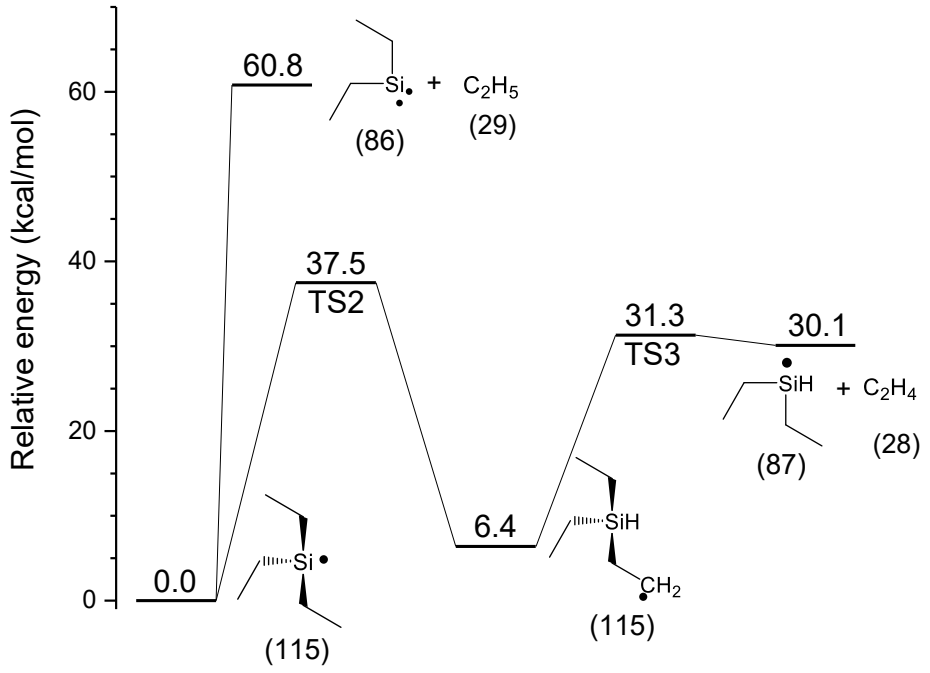

Figure 6. Energetics (0 K) of the dissociation channels of $SiEt_3$ at the UM06-2X/6-311++G(3df, 2pd)//UB3LYP/6-31+G(d,p) level.

shows that the *β*-hydride elimination reaction of $SiEt_3$ is energetically favored. The TST and VTST methods were applied to calculate the unimolecular rate constants of these two competing reaction pathways at different temperatures. As shown in Figure 7, the unimolecular rate constant for the *β*-hydride elimination channel (energetically favored via a tight TS) is larger than that of the C_2H_5 loss channel (energetically less favored via a loose TS). For example, at 1050 K, the rate constant for the *β*-hydride elimination channel is 1.8×10^5 s^{-1}, more than 1 order of magnitude higher than that of the C_2H_5 loss channel (7.6×10^3 s^{-1}). As the temperature further increased, the difference between the two rate constants became smaller. When the temperature reached 1330 K, the calculated rate constant for the *β*-hydride elimination channel of $SiEt_3$ (9.1×10^6 s^{-1}) is larger than that of the C_2H_5 loss channel (2.0×10^6 s^{-1}) by a factor of 4.5. It is then concluded that, around the onset temperature, thermal dissociation of $SiEt_3$ proceeded predominantly via the *β*-hydride elimination channel, and at higher temperatures, the C_2H_5 loss channel became significant. This

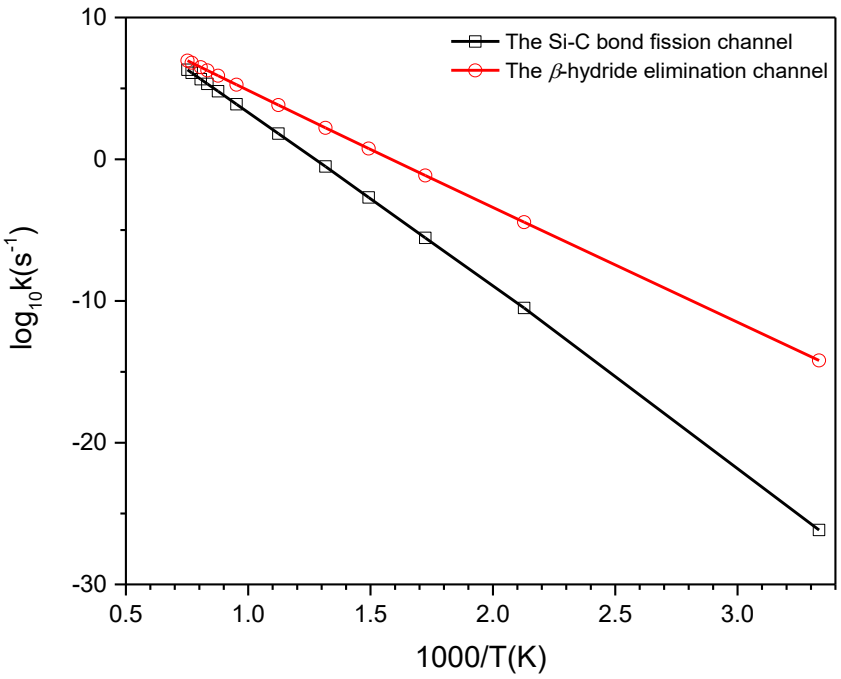

Figure 7. Unimolecular rate constant calculations of the triethylsilyl radical ($SiEt_3$) using the TST/VTST method. The results are displayed in the form of $\log_{10}k$ vs 1000/T.

could explain the first appearance of the m/z = 86 signal at 1200 K, since its bond homolysis rate constant (2.1×10^5 s^{-1}) is only an order magnitude smaller than that of the β-hydride elimination channel (1.8×10^6 s^{-1}).

3. Other important secondary reactions in the tetraethylsilane pyrolysis system.

(1) The secondary reactions of $HSiEt_2$.

Evidence for the appearance of other secondary reactions were also identified. As shown in Figure 2, the signal of m/z = 59 (H_2SiEt) was first observed at 1050 K, and its intensity started to increase until the temperature reached 1200 K, then gradually disappeared as the temperature further increased. Based on the earlier discussion, because the production of $HSiEt_2$ (m/z = 87) became significant at 1050 K and the appearance of the m/z = 59 peak was prior to the signals of

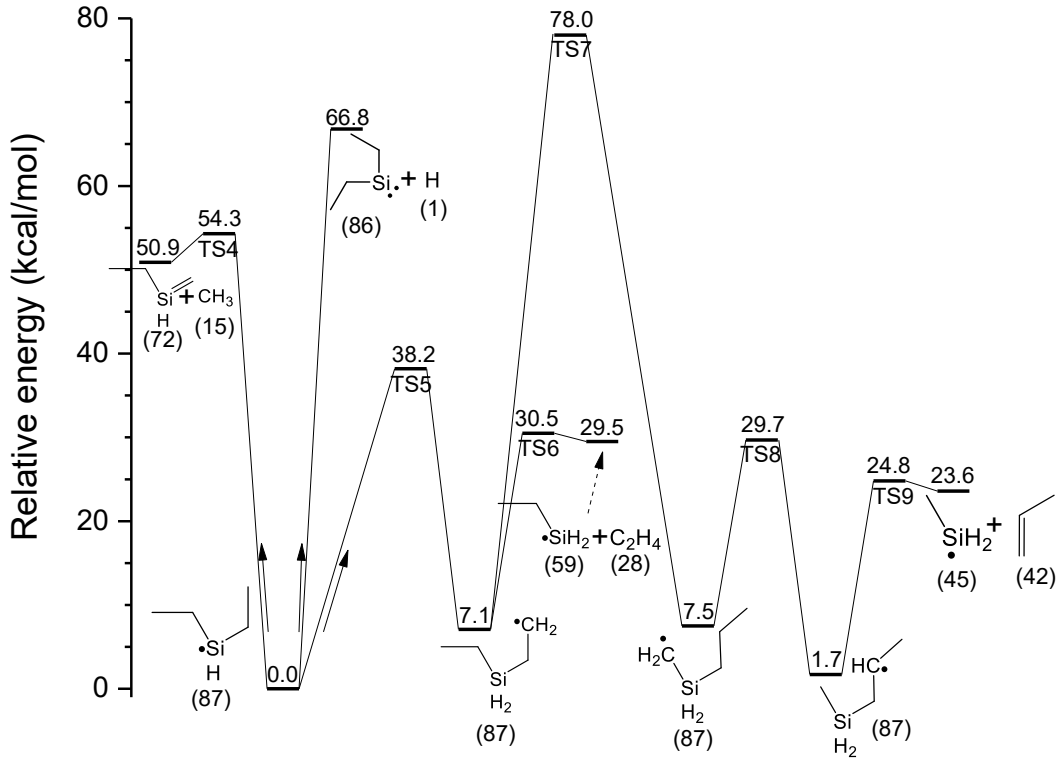

Figure 8. Energetics (0 K) of the possible decomposition channel of $HSiEt_2$ at the UM06-2X/6-311++G(3df, 2pd)//UB3LYP/6-31+G(d,p) level.

other fragment peaks, it is postulated that H_2SiEt was produced from secondary dissociation of $HSiEt_2$. Theoretical calculation regarding the energetics of the dissociation channels of $HSiEt_2$ is shown in Figure 8. As suggested by the DFT calculations, the dissociation of $HSiEt_2$ leading to the production of H_2SiEt (reaction (11)) was similar to the production of $HSiEt_2$ from $SiEt_3$ (reaction (8)) via the β-hydride elimination mechanism. $HSiEt_2$ first isomerized to $H_2SiEtC_2H_4$ with an energy barrier (TS5) of 38.2 kcal/mol, followed by further decomposition to H_2SiEt and C_2H_4 via TS6 with an energy barrier of 23.4 kcal/mol (with respect to $H_2SiEtC_2H_4$).

$$HSiEt_2 \rightarrow H_2SiEtC_2H_4 \rightarrow H_2SiEt + C_2H_4 \quad (11)$$

Figure 8 also indicated a direct decomposition pathway of $HSiEt_2$ that produces $EtHSi{=}CH_2$ and CH_3 (reaction (12)) via TS4, with an energy barrier of 54.3 kcal/mol. This possible reaction pathway was supported by the experimental observations. At 1140 K, the signal of m/z = 72, and m/z = 68 (SiC_3H_4) was first observed. When the temperature further increased, the signal of the m/z = 72 peak remained nearly constant, while the signal intensity of the m/z = 68 peak kept increasing. Earlier studies have established that the detection of the m/z = 68 signals signifies the formation of dimethylsilene ($Me_2Si{=}CH_2$) (m/z = 72) and its isomers such as $EtHSi{=}CH_2$, as dimethylsilene ($Me_2Si{=}CH_2$) can readily undergo thermal decomposition to the neutral m/z = 68 species under the comparable reaction conditions.[33, 34, 39, 59] It is noted that the dimerization of $Me_2Si{=}CH_2$, which could lead to the production of 1,1,3,3-tetramethyl-1,3-disilacyclobutane (m/z = 144) as reported by Tong et al.,[60] could not be confirmed in this study due to overlap of the resulting signal with that of the parent molecule $SiEt_4$; and this dimerization process was unlikely under the current experimental conditions (very short residence and time and low concentrations). Furthermore, as the co-product of $EtHSi{=}CH_2$, the signal of the methyl radical (m/z = 15) was also first observed at 1140 K. Therefore, it is argued that the secondary reaction of $HSiEt_2$ led to the production of $EtHSi{=}CH_2$ and CH_3 from around 1140 K and on. The signal of m/z = 73 (SiC_3H_9) also first appeared at 1140 K, and the origin of this peak was unclear. As previous studies inferred that the ionization cross section of the m/z = 73 species is large,[34, 39, 61] its barely detectable peak intensity suggested that the m/z = 73 species was negligible in the system. Also, quantum chemistry calculation did not demonstrate any possible unimolecular dissociation channel that could explain the appearance of the m/z = 73 signal.

$$HSiEt_2 \rightarrow EtHSi{=}CH_2 + CH_3 \qquad (12)$$

Theoretical calculations may provide a plausible explanation for the H_2SiCH_3 (m/z = 45) production in the secondary reactions of $HSiEt_2$. According to Figure 2, the m/z = 45 signal was first detected at 1140 K, and as the temperature further increased, its peak intensity kept increasing until 1300 K, and then started to decrease. The DFT calculations indicated that the formation of the m/z = 45 species involved a series of isomerization of $HSiEt_2$, followed by a Si-C homolysis. As shown in Figure 8, $HSiEt_2$ first isomerizes to $H_2Si(C_3H_6)CH_3$ via two transition states, TS7 and TS8, and their energy barriers were determined to be 70.9 kcal/mol and 22.2 kcal/mol. Finally, $H_2Si(C_3H_6)CH_3$ overcomes an energy barrier of 23.1 kcal/mol via TS9, leading to the formation of H_2SiCH_3 (m/z = 45) and C_3H_6 (m/z = 42). The signal for the counterpart of H_2SiCH_3 in this reaction (C_3H_6 m/z = 42), however, was not observed simultaneously at 1140 K. The ionization potential of C_3H_6 is 9.73 eV,[62] which is lower than the VUV photon energy used in this work. Therefore, the missing of the m/z = 42 signal indicated the absence of the C_3H_6 species at 1140 K, and thus, it could not support the proposed mechanism. The relatively high energy barrier for TS7 (78.0 kcal/mol relative to $HSiEt_2$) also suggests that there might be an alternative route for the formation of the m/z = 45 signal, which has not been identified yet.

Besides, as shown in Figure 8, the H-loss of $HSiEt_2$ may contribute to the formation of the m/z = 86 ($:SiEt_2$) signal, with an energy threshold of 66.8 kcal/mol. As discussed above, $:SiEt_2$ could be produced from reaction (10) directly at around 1200 K. Alternatively the H-loss channel of $HSiEt_2$ may offer another possible reaction route for the formation of the m/z = 86 species.

(2) The secondary reactions of $:SiEt_2$.

The possible secondary reactions of $:SiEt_2$ (m/z = 86) were also discovered in this work. $:SiEt_2$ may undergo a series of isomerization reactions and lead to the production of the m/z

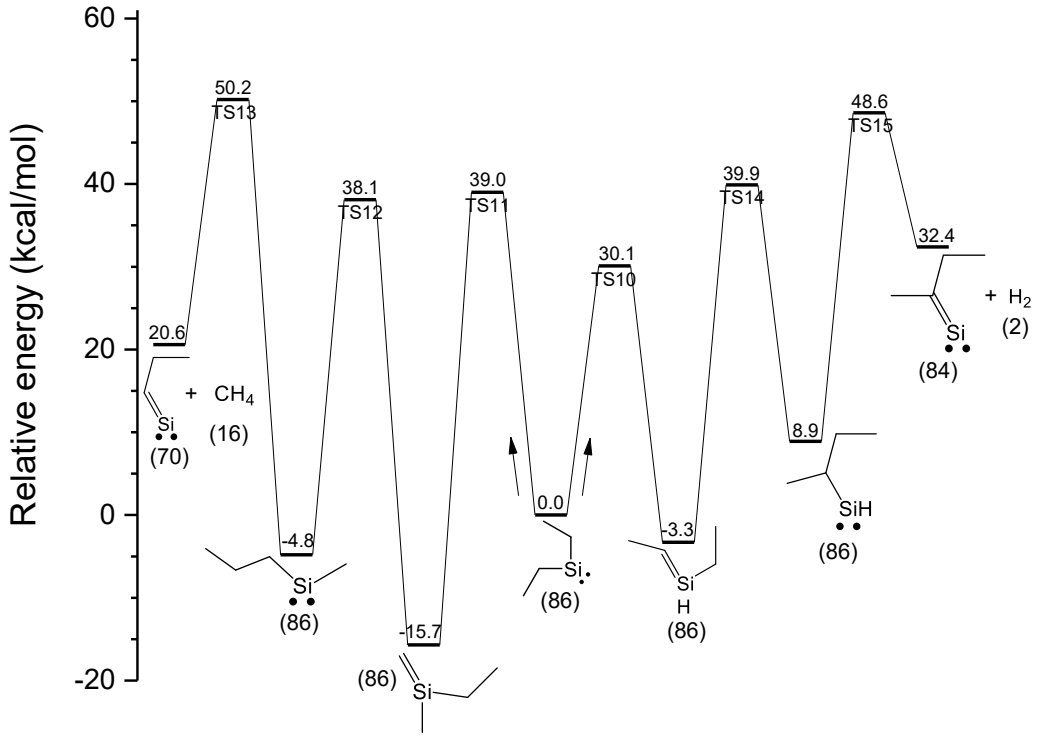

Figure 9. Energetics (0 K) of the possible decomposition channel of :$SiEt_2$ at the UM06-2X/6-311++G(3df, 2pd)//UB3LYP/6-31+G(d,p) level.

= 84 species. As discussed earlier, :$SiEt_2$ could be one of the products of the secondary reactions of $SiEt_3$, and the reaction rate constant calculations suggests that this reaction pathway became significant at high temperatures. After the first appearance of the m/z = 86 peak at 1200 K, the signal of the m/z = 84 peak was first observed at 1240 K. As the temperature further increased, the signal of the m/z = 84 peak remained nearly unchanged until 1330 K. Theoretical calculations regarding a possible two-step mechanism of its formation were carried out, and the energy diagram is shown in Figure 9. According to Figure 9, it was suggested that :$SiEt_2$ first went through an isomerization pathway (TS10) leading to the production of $EtHSi{=}CHCH_3$ with an energy barrier of 30.1 kcal/mol, followed by another isomerization reaction via TS14 forming :$Si(H)CH(Et)CH_3$ with a threshold energy of 43.2 kcal/mol. Finally, :$Si(H)CH(Et)CH_3$ went through a H_2 elimination

mechanism (TS15) to produce :Si=C(Et)CH_3 (m/z = 84), with a calculated energy barrier of 39.7 kcal/mol with respect to :Si(H)CH(Et)CH_3 (reaction (13)).

Theoretical calculations also revealed other possible dissociation channels of :$SiEt_2$. As shown in Figure 9, :$SiEt_2$ could undergo a two-step isomerization reaction through an intermediate CH_2=Si(Et)CH_3 to :Si(CH_3)C_3H_7 via TS11 and TS12, and the overall energy barrier was determined to be 39.0 kcal/mol. Then it could further lose one CH_4 to form :Si=CHC_2H_5 (m/z = 70) over an energy barrier of 55.0 kcal/mol (reaction (14)). This mechanism is consistent with the experimental observations, since at 1240 K the signal of m/z = 70 was found, although, as discussed earlier, the appearance of the m/z = 70 peak could be evolved from the secondary reactions of the m/z = 72 species. As the overall energy barrier of reaction (14) with respect to :$SiEt_2$ (50.2 kcal/mol) is close to that for reaction (13) (48.6 kcal/mol), the contribution for m/z = 70 signal from the secondary reactions of :$SiEt_2$ may not be neglected.

$$SiEt_2 \rightleftharpoons EtHSi{=}CHCH_3 \rightleftharpoons Si(H)CH(Et)CH_3 \rightarrow Si{=}C(Et)CH_3 + H_2 \quad (13)$$

$$SiEt_2 \rightleftharpoons CH_2{=}Si(Et)CH_3 \rightleftharpoons Si(CH_3)C_3H_7 \rightarrow Si{=}CHC_2H_5 + CH_4 \quad (14)$$

(3) The further dissociation reactions of H_2SiEt.

Several possible dissociation channels for H_2SiEt were found in this work. The signal of SiH_3 (m/z = 31) were first found at 1140 K, and its peak intensity kept nearly constant until the temperature reached 1330 K. This was believed to be a secondary reaction product of H_2SiEt. The DFT calculations for the possible dissociation channels is summarized in Figure 10. The reaction pathway that leads to the production of the m/z = 31 peak was the most energetically favored. In this pathway, H_2SiEt first isomerizes to $H_3SiC_2H_4$ via TS16 with an energy barrier of 38.7 kcal/mol.

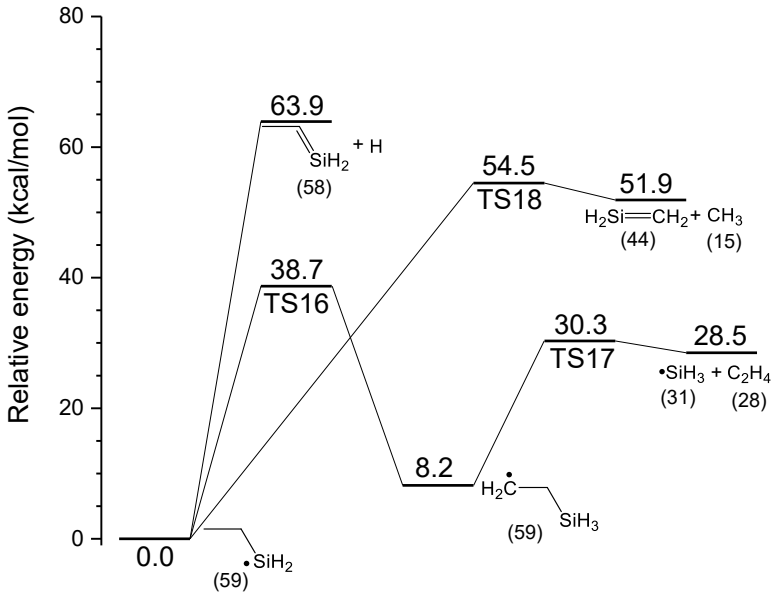

Figure 10. Energetics (0 K) of the possible decomposition channel of H_2SiEt at the UM06-2X/6-311++G(3df, 2pd)//UB3LYP/6-31+G(d,p) level.

Then $H_3SiC_2H_4$ decomposes to SiH_3 and C_2H_4 via TS17 with an energy barrier of 22.1 kcal/mol (relative to $H_3SiC_2H_4$).

Theoretical calculations also indicates that H_2SiEt could further decompose into $H_2Si{=}CH_2$ and CH_3 via TS18, with an energy barrier of 54.5 kcal/mol. The experimental observations are consistent with this proposed mechanism as the signal of the m/z = 44 species was first detected at 1200 K. Its later appearance than the m/z = 31 is also consistent with the theoretical calculations that the energy barrier for TS18 is higher than that for TS16.

H_2SiEt could further lose a hydrogen atom forming $H_2Si{=}CHCH_3$ (m/z = 58). As shown in Figure 2, the m/z = 58 signal first showed up at 1240 K and remained nearly constant when the temperature further increased. One explanation for this peak is the H-loss reaction of H_2SiEt. Figure 10 displays that the energy threshold for this reaction is 63.9 kcal/mol, which is higher than the other two reaction pathways of H_2SiEt. Experimental observations agreed with this calculation

results, since the temperature for the first appearance of m/z = 58 is higher than those of other two reaction pathways.

(4) Other possible secondary reaction channels.

When the pyrolysis temperature further increased, more fragment signals appeared, and the fragment signal from m/z = 54 – 57 were possibly yielded from the secondary reactions of the m/z = 58 species ($H_2Si{=}CHCH_3$). For example, as shown in Figure 2, the signal of the m/z = 57 and 56 species first showed up at 1240 K, and these two peaks were possibly the dissociation reaction products of the m/z = 58 species discussed earlier. Their possible dissociation reaction energetics were calculated theoretically and are displayed in Figure 11. Figure 11 suggests that there may be

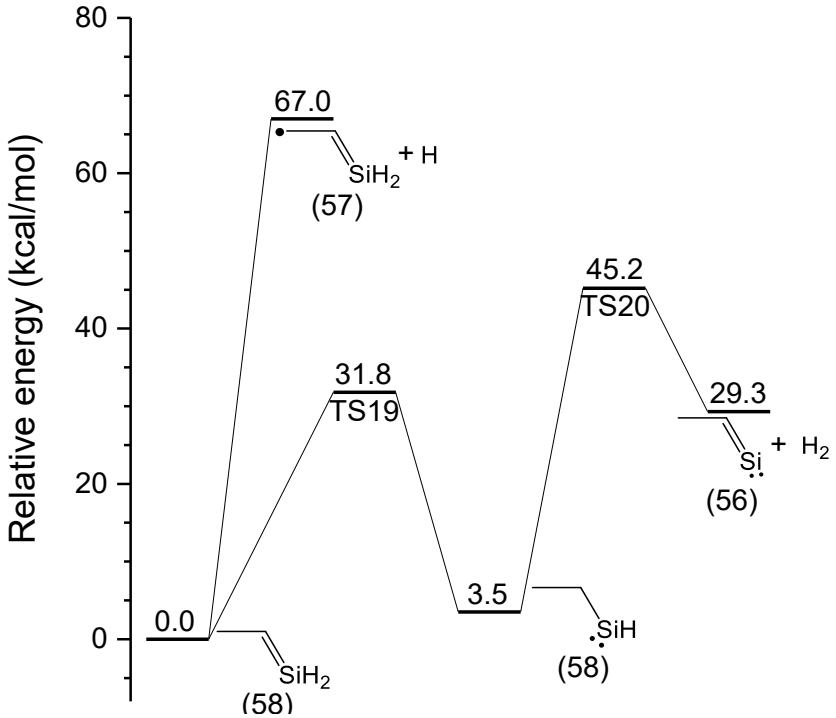

Figure 11. Energetics (0 K) of the possible decomposition channel of the m/z = 58 species at the UM06-2X/6-311++G(3df, 2pd)//UB3LYP/6-31+G(d,p) level.

an isomerization reaction channel between $H_2Si=CHCH_3$ and :SiHEt via TS19 with an energy barrier of 31.8 kcal/mol. The m/z = 56 species ($:Si=CHCH_3$) was possibly caused by H_2 elimination reaction of :SiHEt, via TS20 with an energy barrier of 41.7 kcal/mol. As the temperature increased to 1300 K, the m/z = 54 signal first appeared; it might correspond to $:Si=C=CH_2$, possibly produced from further H_2 elimination reactions of $:Si=CHCH_3$. The m/z = 57 species were probably produced from the H-loss reaction of $H_2Si=CHCH_3$, with an energy threshold of 67.0 kcal/mol.

The m/z = 43 and 42 signal were also captured in this work. When the temperature reached 1200 K, the m/z = 43 and 42 signal first appeared. Unlike the m/z = 44 signal, the intensity for the m/z = 43 and 42 signal kept increasing when the temperature further increased. It was possibly caused by further dissociations of the m/z = 44 species. Previous studies have discussed the secondary reactions of the m/z = 44 species in detail; the m/z = 44 species could lose H or H_2, and lead to the production of the $SiCH_3$ (m/z = 43) or $SiCH_2$ (m/z = 42) species.[39] Also, the m/z = 44 – 42 signals could correspond to signals of hydrocarbons (C_3H_8 – C_3H_6) from multiple secondary reactions, and it could be further identified by structural studies in the future.

Conclusion

The thermal decomposition of tetraethylsilane was investigated experimentally by using flash pyrolysis vacuum ultraviolet mass spectrometry. DFT calculations regarding the energetics of the initiation reactions and important secondary reactions were performed. In the initiation step of the tetraethylsilane pyrolysis, the Si-C bond homolysis was found to be the predominant reaction pathway, with $SiEt_3$ as the primary dissociation product, instead of the direct β-hydride elimination pathway. The unimolecular rate constant calculations with the TST and VTST methods revealed that the rate constant of the Si-C bond fission channel was 5 orders magnitude higher than the β-

hydride elimination pathway. In the secondary dissociation pathways of $SiEt_3$, however, the β-hydride elimination pathway producing $HSiEt_2$ was predominant at lower temperatures than the Si-C bond fission (producing $:SiEt_2$); while at higher temperatures, the Si-C bond homolysis became more significant.

Several secondary reactions were identified in the tetraethylsilane pyrolysis. The further dissociation reaction of $HSiEt_2$ was believed to be associated with the appearance of the m/z = 59 species (H_2SiEt); also, possible dissociation channels of $HSiEt_2$ leading to the productions of the m/z = 72 species and the m/z = 45 species were proposed. The secondary reactions of $:SiEt_2$ that led to the formation of the m/z = 84 species and m/z = 70 species were described. Other possible secondary reaction channels that involved in this work, such as the production of the m/z = 54 – 57 species and m/z = 44 – 42 species, were also discussed. The main thermal decomposition mechanism of tetraethylsilane, including the initiation reaction channels and several important secondary reaction pathways, are summarized in Scheme 1.

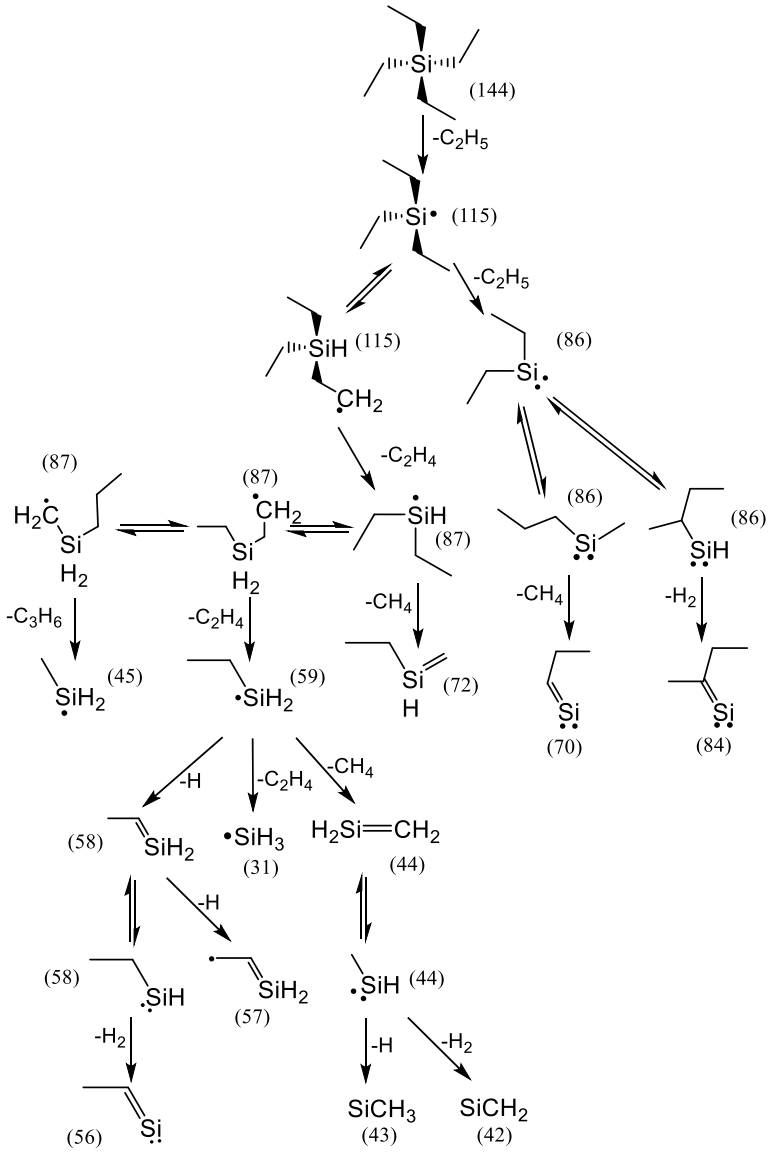

Scheme 1. Main thermal decomposition mechanism of the pyrolysis of tetraethylsilane.

Supporting Information

Additional computational details, including geometries of the reactant, transition states, reactive intermediates, and products involved in the $SiEt_4$ system; geometries and frequencies of species involved in the TST/VTST unimolecular reaction rate constant calculations; and the calculated unimolecular rate constants for the relevant reaction channels at various temperatures.

Acknowledgement

This work was supported by the US National Science Foundation (NSF CHE-2155232). KLS acknowledges support from a UC President's Dissertation-Year Fellowship. XHL acknowledges support of a scholarship from China Scholarships Council (201606440042).

Declaration of Conflicting Interests Statement

The Authors declare that there is no conflict of interest.

Reference

(1) Sun, L.; Yuan, G.; Gao, L.; Yang, J.; Chhowalla, M.; Gharahcheshmeh, M. H.; Gleason, K. K.; Choi, Y. S.; Hong, B. H.; Liu, Z. Chemical vapour deposition. *Nature Reviews Methods Primers* **2021**, *1* (1), 5.

(2) Mohd Sohor, M. A. H.; Mustapha, M.; Chandra Kurnia, J. Silicon carbide- from synthesis to application: a review. *MATEC Web Conf.* **2017**, *131*, 04003.

(3) Hotza, D.; Di Luccio, M.; Wilhelm, M.; Iwamoto, Y.; Bernard, S.; Diniz da Costa, J. C. Silicon carbide filters and porous membranes: A review of processing, properties, performance and application. *Journal of Membrane Science* **2020**, *610*, 118193.

(4) Davis, R. F.; Kelner, G.; Shur, M.; Palmour, J. W.; Edmond, J. A. Thin film deposition and microelectronic and optoelectronic device fabrication and characterization in monocrystalline alpha and beta silicon carbide. *Proceedings of the IEEE* **1991**, *79* (5), 677-701.

(5) Selvakumar, J.; Sathiyamoorthy, D. Prospects of chemical vapor grown silicon carbide thin films using halogen-free single sources in nuclear reactor applications: A review. *Journal of Materials Research* **2012**, *28* (1), 136-149, From Cambridge University Press Cambridge Core.

(6) Lemieux, J. M.; Zhang, J. Thermal decomposition of tetramethylsilane and tetramethylgermane by flash pyrolysis vacuum ultraviolet photoionization time-of-flight mass spectrometry. *International Journal of Mass Spectrometry* **2014**, *373*, 50-55.

(7) Kim, K. C.; Nahm, K. S.; Hahn, Y. B.; Lee, Y. S.; Byun, H.-S. Kinetic study of 3C-SiC growth on Si by pyrolyzing tetramethysilane in low pressure radio frequency-induction heated chemical vapor deposition reactor. *Journal of Vacuum Science & Technology A* **2000**, *18* (3), 891-899.

(8) Golecki, I.; Reidinger, F.; Marti, J. Single‐crystalline, epitaxial cubic SiC films grown on (100) Si at 750 °C by chemical vapor deposition. *Applied Physics Letters* **1992**, *60* (14), 1703-1705.

(9) Veneroni, A.; Omarini, F.; Masi, M. Silicon carbide growth mechanisms from SiH_4, $SiHCl_3$ and nC_3H_8. *Crystal Research and Technology* **2005**, *40* (10-11), 967-971.

(10) Badran, I.; Shi, Y. A kinetic study of the gas-phase reactions of 1-methylsilacyclobutane in hot wire chemical vapor deposition. *Physical Chemistry Chemical Physics* **2018**, *20* (1), 75-85, 10.1039/C7CP06082C.

(11) Lemieux, J. M.; Zhang, J. Letter: Thermal decomposition of methyltrichlorosilane, dimethyldichlorosilane and methyldichlorosilane by flash pyrolysis vacuum ultraviolet

photoionization time-of-flight mass spectrometry. *European Journal of Mass Spectrometry* **2014**, *20* (5), 409-417.

(12) Wrobel, A. M.; Walkiewicz-Pietrzykowska, A.; Ahola, M.; Vayrynen, I. J.; Ferrer-Fernandez, F. J.; Gonzalez-Elipe, A. R. Growth mechanism and chemical structure of amorphous hydrogenated silicon carbide (a-SiC:H) films formed by remote hydrogen microwave plasma CVD from a triethylsilane precursor: Part 1. *Chemical Vapor Deposition* **2009**, *15* (1-3), 39-46.

(13) Keister, J. W.; Tomperi, P.; Baer, T. Thermochemistry of gaseous ethylsilanes and their radical cations. *Journal of the American Society for Mass Spectrometry* **1998**, *9* (6), 597-605.

(14) Maya, L. Deposition of a-SiC:H using organosilanes in an argon/hydrogen plasma. *MRS Online Proceedings Library* **1993**, *327* (1), 215-220.

(15) Zaitseva, N.; Hamel, S.; Dai, Z. R.; Saw, C.; Williamson, A.; Galli, G. Effect of nitrogen on the stability of silicon nanocrystals produced by decomposition of alkyl silanes. *The Journal of Physical Chemistry C* **2008**, *112* (10), 3585-3590.

(16) Amjoud, M. b.; Reynes, A.; Morancho, R.; Carles, R. Comparative study of decomposition by metal-organic chemical vapour deposition of tetraethylsilane and tetravinylsilane. *Journal of Materials Chemistry* **1992**, *2* (11), 1205-1208, 10.1039/JM9920201205.

(17) Vandenbulke, L.; Leparoux, M. Silicon and boron containing components by CVD and CVI for high temperature ceramic composites. *J. Phys. IV France* **1995**, *05* (C5), C5-735-C735-751.

(18) Lee, D. C.; Hanrath, T.; Korgel, B. A. The role of precursor-decomposition kinetics in silicon-nanowire synthesis in organic solvents. *Angewandte Chemie International Edition* **2005**, *44* (23), 3573-3577.

(19) Asahina, S.; Kubo, N.; Tsuda, H.; Kanayama, N.; Moritani, A.; Kitahara, K. Crystalline structure of SiC thin films grown by MOCVD method with tetraethylsilane. *Journal of The Surface Finishing Society of Japan* **2003**, *54* (5), 372-373.

(20) Pola, J.; Parsons, J. P.; Taylor, R. ArF laser photolysis of tetraethyl- and tetravinyl-silane. *Journal of Organometallic Chemistry* **1995**, *489* (1), C9-C11.

(21) Ring, M. A.; O'Neal, H. E.; Rickborn, S. F.; Sawrey, B. A. Kinetics of the high-temperature thermal decomposition of silanes and alkylsilanes. *Organometallics* **1983**, *2* (12), 1891-1894.

(22) Rickborn, S. F.; Ring, M. A.; O'Neal, H. E. The kinetics and mechanism of the shock induced gas phase decomposition of ethylsilane. *International Journal of Chemical Kinetics* **1984**, *16* (11), 1371-1383.

(23) Jardine, R. E.; O'Neal, H. E.; Ring, M. A.; Beatie, M. E. Mechanism of the thermal decomposition of ethylsilane. *The Journal of Physical Chemistry* **1995**, *99* (33), 12507-12511.

(24) Sela, P.; Peukert, S.; Somnitz, H.; Janbazi, H.; Wlokas, I.; Herzler, J.; Fikri, M.; Schulz, C. Kinetics of the thermal decomposition of ethylsilane: shock-tube and modeling study. *Energy & Fuels* **2021**, *35* (4), 3266-3282.

(25) Martin, J. G.; Ring, M. A.; O'Neal, H. E. The decomposition kinetics of disilane and the heat of formation of silylene. *International Journal of Chemical Kinetics* **1987**, *19* (8), 715-724.

(26) Coon, P. A.; Wise, M. L.; George, S. M. Adsorption kinetics for ethylsilane, diethylsilane, and diethylgermane on Si(111) 7×7. *The Journal of Chemical Physics* **1993**, *98* (9), 7485-7495.

(27) Keeling, L. A.; Chen, L.; Michael Greenlief, C.; Mahajan, A.; Bonser, D. Direct evidence for β-hydride elimination on Si (100). *Chemical Physics Letters* **1994**, *217* (1), 136-141.

(28) Dillon, A. C.; Robinson, M. B.; Han, M. Y.; George, S. M. Diethylsilane decomposition on silicon surfaces studied using transmission FTIR spectroscopy. *Journal of The Electrochemical Society* **1992**, *139* (2), 537-543.

(29) Foster, M.; Darlington, B.; Scharff, J.; Campion, A. Surface chemistry of alkylsilanes on Si(100)2 × 1. *Surface Science* **1997**, *375* (1), 35-44.

(30) Chambreau, S. D.; Zhang, J.; Traeger, J. C.; Morton, T. H. Photoionization of methyl t-butyl ether (MTBE) and t-octyl methyl ether (TOME) and analysis of their pyrolyses by supersonic jet/photoionization mass spectrometry. *International Journal of Mass Spectrometry* **2000**, *199* (1), 17-27.

(31) Chambreau, S. D.; Zhang, J. VUV photoionization time-of-flight mass spectrometry of flash pyrolysis of silane and disilane. *Chemical Physics Letters* **2001**, *343* (5), 482-488.

(32) Shao, K.; Liu, X.; Jones, P. J.; Sun, G.; Gomez, M.; Riser, B. P.; Zhang, J. Thermal decomposition of cyclohexane by flash pyrolysis vacuum ultraviolet photoionization time-of-flight mass spectrometry: a study on the initial unimolecular decomposition mechanism. *Physical Chemistry Chemical Physics* **2021**, *23* (16), 9804-9813, 10.1039/D1CP00459J.

(33) Liu, X.; Zhang, J.; Vazquez, A.; Wang, D.; Li, S. Mechanism of the thermal decomposition of tetramethylsilane: a flash pyrolysis vacuum ultraviolet photoionization time-of-flight mass spectrometry and density functional theory study. *Physical Chemistry Chemical Physics* **2018**, *20* (27), 18782-18789, 10.1039/C8CP02626B.

(34) Shao, K.; Tian, Y.; Zhang, J. Thermal decomposition mechanism of allyltrichlorosilane and allyltrimethylsilane. *International Journal of Mass Spectrometry* **2021**, *460*, 116476.

(35) Jones, P. J.; Riser, B.; Zhang, J. Flash pyrolysis of t-butyl hydroperoxide and di-t-butyl peroxide: evidence of roaming in the decomposition of organic hydroperoxides. *The Journal of Physical Chemistry A* **2017**, *121* (41), 7846-7853.

(36) Kohn, D. W.; Clauberg, H.; Chen, P. Flash pyrolysis nozzle for generation of radicals in a supersonic jet expansion. *Review of Scientific Instruments* **1992**, *63* (8), 4003-4005.

(37) Guan, Q.; Urness, K. N.; Ormond, T. K.; David, D. E.; Barney Ellison, G.; Daily, J. W. The properties of a micro-reactor for the study of the unimolecular decomposition of large molecules. *International Reviews in Physical Chemistry* **2014**, *33* (4), 447-487.

(38) Zagidullin, M. V.; Kaiser, R. I.; Porfiriev, D. P.; Zavershinskiy, I. P.; Ahmed, M.; Azyazov, V. N.; Mebel, A. M. Functional relationships between kinetic, flow, and geometrical parameters in a high-temperature chemical microreactor. *The Journal of Physical Chemistry A* **2018**, *122* (45), 8819-8827.

(39) Shao, K.; Tian, Y.; Zhang, J. A mechanistic study of thermal decomposition of 1,1,2,2-tetramethyldisilane using vacuum ultraviolet photoionization time-of-flight mass spectrometry. *The Journal of Physical Chemistry A* **2022**, *126* (7), 1085-1093.

(40) Frisch, M. J.; Trucks, G. W.; Schlegel, H. B.; Scuseria, G. E.; Robb, M. A.; Cheeseman, J. R.; Scalmani, G.; Barone, V.; Petersson, G. A.; Nakatsuji, H.; et al., *Gaussian 16 Rev. C.01*; Wallingford, CT, 2016.

(41) Tentscher, P. R.; Arey, J. S. Geometries and vibrational frequencies of small radicals: Performance of coupled cluster and more approximate methods. *Journal of Chemical Theory and Computation* **2012**, *8* (6), 2165-2179.

(42) Brémond, É.; Savarese, M.; Su, N. Q.; Pérez-Jiménez, Á. J.; Xu, X.; Sancho-García, J. C.; Adamo, C. Benchmarking density functionals on structural parameters of small-/medium-sized organic molecules. *Journal of Chemical Theory and Computation* **2016**, *12* (2), 459-465.

(43) Khanal, G. P.; Parajuli, R.; Arunan, E.; Yamabe, S.; Hiraoka, K.; Torikai, E. Study of structures, energies and vibrational frequencies of $(O_2)_n^+$ (n=2–5) clusters by GGA and meta-GGA density functional methods. *Computational and Theoretical Chemistry* **2015**, *1056*, 24-36.

(44) Zhao, Y.; Truhlar, D. G. The M06 suite of density functionals for main group thermochemistry, thermochemical kinetics, noncovalent interactions, excited states, and transition elements: two new functionals and systematic testing of four M06-class functionals and 12 other functionals. *Theoretical Chemistry Accounts* **2008**, *120* (1), 215-241.

(45) Truhlar, D. G.; Garrett, B. C.; Klippenstein, S. J. Current Status of Transition-State Theory. *The Journal of Physical Chemistry* **1996**, *100* (31), 12771-12800.

(46) Wigner, E. The transition state method. *Transactions of the Faraday Society* **1938**, *34* (0), 29-41, 10.1039/TF9383400029.

(47) Canneaux, S.; Bohr, F.; Henon, E. KiSThelP: A program to predict thermodynamic properties and rate constants from quantum chemistry results†. *Journal of computational chemistry* **2014**, *35* (1), 82-93.

(48) Jasper, A. W.; Miller, J. A.; Klippenstein, S. J. Collision Efficiency of Water in the Unimolecular Reaction CH_4 (+H_2O) ⇆ CH_3 + H (+H_2O): One-Dimensional and Two-Dimensional Solutions of the Low-Pressure-Limit Master Equation. *The Journal of Physical Chemistry A* **2013**, *117* (47), 12243-12255.

(49) NIST Computational Chemistry Comparison and Benchmark Database. NIST Standard Reference Database Number 101, Release 22, May 2022, Editor: Russell D. Johnson III http://cccbdb.nist.gov/. (accessed May 18, 2022).

(50) Ali, M. A. Computational studies on the gas phase reaction of methylenimine (CH_2NH) with water molecules. *Scientific Reports* **2020**, *10* (1), 10995.

(51) Shao, K.; Brunson, J.; Tian, Y.; Zhang, J. Flash pyrolysis mechanism of trimethylchlorosilane. *International Journal of Mass Spectrometry* **2022**, *482*, 116933.

(52) Mohandas, S.; Ramabhadran, R. O.; Kumar, S. S. Theoretical Investigation of a Vital Step in the Gas-Phase Formation of Interstellar Ammonia $NH_2^+ + H_2 \rightarrow NH_3^+ + H$. *The Journal of Physical Chemistry A* **2020**, *124* (41), 8373-8382.

(53) Begum, S.; Subramanian, R. Theoretical studies on gas-phase kinetics and mechanism of H-abstraction reaction from methanol by ClO and BrO radicals. *RSC Advances* **2015**, *5* (49), 39110-39121, 10.1039/C5RA06483J.

(54) Meija, J.; Coplen Tyler, B.; Berglund, M.; Brand Willi, A.; De Bièvre, P.; Gröning, M.; Holden Norman, E.; Irrgeher, J.; Loss Robert, D.; Walczyk, T.; et al. Atomic weights of the elements 2013 (IUPAC Technical Report). *pac* **2016**, *88* (3), 265-291.

(55) Li, X. M.; Eustergerling, B. D.; Shi, Y. J. Mass spectrometric study of gas-phase chemistry in a hot-wire chemical vapor deposition reactor with tetramethylsilane. *International Journal of Mass Spectrometry* **2007**, *263* (2), 233-242.

(56) Amaral, G.; Xu, K.; Zhang, J. UV photodissociation dynamics of ethyl radical via the Ã2A′ (3s) state. *The Journal of Chemical Physics* **2001**, *114* (12), 5164-5169.

(57) Weber, K. H.; Lemieux, J. M.; Zhang, J. Flash pyrolysis of ethyl, n-propyl, and isopropyl iodides as monitored by supersonic expansion vacuum ultraviolet photoionization time-of-flight mass spectrometry. *The Journal of Physical Chemistry A* **2009**, *113* (3), 583-591.

(58) Ohno, K.; Okamura, K.; Yamakado, H.; Hoshino, S.; Takami, T.; Yamauchi, M. Penning ionization of HCHO, CH_2CH_2, and CH_2CHCHO by collision with He(2^3S) metastable atoms. *The Journal of Physical Chemistry* **1995**, *99* (39), 14247-14253.

(59) Liu, X.; Zhang, J.; Vazquez, A.; Wang, D.; Li, S. Mechanistic study of thermal decomposition of hexamethyldisilane by flash pyrolysis vacuum ultraviolet photoionization time-of-flight mass spectrometry and density functional theory. *The Journal of Physical Chemistry A* **2019**, *123* (49), 10520-10528.

(60) Tong, L.; Shi, Y. J. A mechanistic study of gas-phase reactions with 1,1,3,3-tetramethyl-1,3-disilacyclobutane in the hot-wire chemical vapor deposition process. *Thin Solid Films* **2009**, *517* (12), 3461-3465.

(61) Kawaguchi, S.; Takahashi, K.; Satoh, K.; Itoh, H. Electron collision cross section sets of TMS and TEOS vapours. *Plasma Sources Science and Technology* **2017**, *26* (5), 054001.

(62) Traeger, J. C. A study of the allyl cation thermochemistry by photoionization mass spectrometry. *International Journal of Mass Spectrometry and Ion Processes* **1984**, *58*, 259-271.

TOC Graphic